DYNAMIC FRACTURE OF ARMOR STEEL

B. Gailly* and A. Pineau**

Armor steels become harder and harder. Unfortunately this increase of strength induces brittleness, and fracture occurs during penetration of projectiles. The purpose of the present paper is to study the dynamic fracture of a very high strength 0.5% C martensitic armor steel (UTS=2300 MPa, K_{Ic}=50 MPa$\sqrt{m}$) showing a ductile fracture mode while the crack aspect is brittle. The fracture toughness at crack initiation, K_{Ic}, and at crack arrest, K_{Ia}, have been measured with a new ring specimen geometry and compared to the values obtained with conventional CT specimens. This geometry has never been used before on specimens showing a ductile fracture mode. The results show that K_{Ia} is independent of the crack velocity over the range between 0.1 and 500 m/s.

INTRODUCTION

In ballistic field armor hardness is a prime characteristic to resist against kinetic projectiles. But this increase in strength is usually accompanied by a decrease in ductility. Therefore the knowledge of their fracture behaviour is very important to understand their ballistic performance. In a previous paper, Gailly and Petit (1) performed plate impact experiments in a spalling configuration to reproduce as well as possible the process involved during projectile penetration. They showed that the spall stress is not a good criterion to characterize the fracture mechanism involved during ballistic impact. However it was shown that it gives valuable information on crack nucleation. Moreover in this study it was observed that the fracture mode remained ductile even at very high velocities. The purpose of this paper is to investigate more deeply crack propagation and crack arrest in a very high strength armor steel. In this study a new ring shape specimen geometry recently developed (Iung (2)) was used. In this geometry the variation of K with crack length follows a bell shape curve. This is useful to investigate both crack

* ETBS Rte de Guerry BP 712 18015 Bourges (France)
** Ecole des Mines BP 87 91003 Evry (France) URACNRS 866

initiation, rapid crack propagation and crack arrest. The ring specimen was initially devised for brittle cleavage fracture. In this study it is applied for the first time to a steel which leads to ductile fracture. A special emphasis is led on the effect of crack velocity on crack arrest fracture toughness.

MATERIALS AND EXPERIMENTAL PROCEDURES

The material studied is a low alloy steel with 0.5%C, called MARS 300, manufactured by Creusot Loire Industrie. It was quenched and tempered below 500°C which leads to a predominant martensitic microstructure with 12% residual austenite. The material, delivered as plates of 40 mm thickness, was rolled along several directions in order to provide isotropic mechanical properties in the plane. The main mechanical properties measured in transverse direction on tensile specimens with a diameter of 4 mm and a gauge length of 20 mm are: Yield strength:1450 MPa, Uniform tensile strength:2275 MPa, Tensile elongation:3.5%.

A sketch of the ring test specimen is shown in Fig. 1. The ring is defined by its external and internal radii, R_2 and R_1. A radial crack of length a is located in the equatorial plane. The geometry is characterized by two parameters :$\beta=R_1/R_2$ and $\lambda=a/(R_2-R_1)$. The dimensions are initially R_1=16.25 mm, R_2=37.5 mm while the thickness, B, is 10 mm. Most specimens were fatigue precracked from a notch, by compressive loading at room temperature. The maximum load applied during precracking was 50 KN. The rings were subsequently machined to their final dimensions: R_2=32.5 mm, R_1=16.25 mm and B=7.50 mm. Three specimens were not fatigue precracked. They contained a sharp notch with a radius of curvature of 0.10 mm. The specimens were submitted to a compressive load P_0 applied at room temperature. In this geometry the stress intensity factor can be written as :

$$K = \frac{P_0}{B\sqrt{R_2}} k(\lambda) \qquad (1)$$

where k is a parameter which is a function of λ (Fig. 1b) taken from (2). The bell shape of this curve is useful to investigate the effect of crack speed on crack arrest behaviour. The crack velocity is simply modified by changing the initial crack length. Small crack lengths will produce increasing crack velocities. This property is largely used in this study. Additional tests containing sharp notches were also carried out to explore a wider range of crack speeds. The crack velocity was measured with gauges glued on the surface of the specimens. They contain wires every 0.25 mm. A high speed oscilloscope triggered by the breaking of one of these wires records the signal used to measure the crack speed. In this specific specimen, elastically very rigid, the load remains constant during crack propagation. This largely facilitates the calculation of K_{Ia}, from Eq. 1, even for very high crack speeds. An extensometer is placed across the crack mouth (Fig. 1a) to measure its opening at crack initiation and crack arrest. After the test the specimens are blue heat tinted and broken to measure carefully the initial and the final crack lengths.

RESULTS AND DISCUSSION

The results of the tests are shown in Table 1 where the initial conditions (crack tip geometry and λ_0) are given. The crack velocities reported in this table were determined from results similar to those shown in Fig. 2 corresponding to test 308. In this figure it is observed that the crack velocity, after a brief acceleration, reaches a maximum value (30 m/s) when λ is close to the maximum of the $k(\lambda)$ curve (Fig. 1b) and then decreases when the crack stops. The values of the crack speed reported in Table 1 are those corresponding to the maximum crack velocity, $\dot{a}_{max}$.

The test results show that the maximum crack velocity is a decreasing function of initial fatigue crack length, $\lambda_0=a_0/(R_2-R_1)$ (Fig. 3). This is simply explained by the fact that the strain energy release rate increases with crack length for small cracks and that this effect is all the more pronounced as the crack length is small. This explanation is consistent with the test 311 carried out on a small notch which led to the largest crack velocity measured in the present study. In this specific case the load at crack initiation was much larger (P=127 KN) than that necessary to initiate fracture from a fatigue crack of similar length.

The values of K_{Ic} reported in Table 1 are similar to those determined on conventional CT specimens for which it was shown (1) that K_{Ic} was equal to 50 MPa$\sqrt{m}$. However K_{Ic} values inferred from these tests on short cracks are systematically lower than those measured on long cracks. The effect is more pronounced in tests 307, 308 and 309. The reasons for this difference are not yet fully understood. The values of K_{Ia} are observed to be independent of the crack velocity or similarly of the initial crack length (Fig. 4). It is noticed that the crack arrest fracture toughness is large even at very high crack speeds (test 311). This behaviour is largely different from the situation which is usually observed for brittle cleavage fracture (3). SEM observations showed that in the present material the fracture mode is ductile with the formation of dimples on the fracture surfaces.

TABLE 1 - Initial conditions and results on ring shape geometry

Specimen	Crack tip radius (mm)	λ_0	P_0 (KN)	K_{Ic} (MPa$\sqrt{m}$)	K_{Ia} (MPa$\sqrt{m}$)	$\dot{a}_{max}$ (m/s)
300	0.1	0.29	100	/	39.7	/
301	fatigue	0.23	70	51	36.7	0.1
302	fatigue	0.15	71.4	46	45.4	0.4
303	fatigue	0.17	68	46	43.5	0.1
307	fatigue	0.05	92.5	38	43.9	100
308	fatigue	0.08	82	42	47.7	30
309	fatigue	0.07	81	40	47.9	9
311	0.1	0.08	127	/	39.0	500
312	0.1	0.08	135	/	35.0	280

This difference in crack arrest behaviour with the failure mode has not yet been reported to the knowledge of the authors. It is worth noting that a similar effect is observed for crack initiation. A number of authors (see eg (2)) have shown that the toughness for ductile fracture is an increasing function of strain rate while it is well known that KId for cleavage fracture is a decreasing function of strain rate (3). This situation which seems to be also observed to some extent for crack arrest is largely related to the fact that ductile fracture is essentially strain-controlled while cleavage fracture is essentially stress-controlled.

An attempt was made to measure the extent of the plastic zone surrounding the propagating cracks. These measurements were made using surface roughness measurements. The results shown in Fig. 5 illustrate a situation typically observed (test 308). The plastic zone size increases after crack initiation to reach a maximum in the vicinity of maximum of the $k(\lambda)$ curve and then decreases progressively. These results are used in Fig. 6 where we have plotted the variation of the plastic zone wake r_p wersus the square of the stress intensity factor calculated with Eq 1. In this figure we have only included the data points corresponding to the region where the crack velocity was maximum, i.e. close to the maximum of the $k(\lambda)$ curve. It is observed that, within a first approximation, r_p is proportional to K^2 as predicted from the well-known expression under plane stress conditions:

$$r_p = \frac{1}{i.\pi}\left(\frac{K}{\sigma_Y}\right)^2 \qquad (2)$$

where σ_Y is the yield strength and i is a factor which differs between authors (see eg (2)). The results of Fig. 6 lead to i=0.7 for the test in which $\dot{a}_{max}$ was of the order of 0.1 m/s, assuming that σ_Y was equal to 1450 MPa (Table 1) which is the static yield strengh measured at $\dot{\varepsilon}=10^{-3}\ s^{-1}$. Plate impact experiments showed that the yield strengh of the material was almost the same at a strain rate of $2.10^5\ s^{-1}$ (4). It seems therefore difficult to invoke a strain rate effect on the yield strength to explain the change in slope of the r_p-K^2 curve with crack speed. However it is difficult to assess accurately the strain rate ahead of a propagating crack. A simple expression was proposed by Di-Fant (5). This expression can be written as :

$$\varepsilon \approx \frac{(1+\nu)(1-2\nu)}{2E}\frac{aK}{\sqrt{2\pi}\ r^{\frac{3}{2}}} \qquad (3)$$

where ν is the Poisson ratio, E the elastic modulus and r the distance from the crack tip. This expression leads to $\dot{\varepsilon}=10^3\ s^{-1}$ for $\dot{a}$=500 m/s and $r=8.10^{-4}$ m which corresponds roughly to the observed plastic zone size and to $\dot{\varepsilon}=10^5\ s^{-1}$ for $r=4.10^5$ m. On the other hand, the results of Fig. 6 obtained at $\dot{a}$=500 m/s are consistent with Eq. 2 in which it is assumed that i=0.7 if the yield strength is assumed to be about 2200 MPa which is much higher than the values determined even at $\dot{\varepsilon}=10^5\ s^{-1}$. This might suggest that the strain rates, within the plastic zone are larger than those inferred from Eq. 3. In particular they might correspond to the viscous flow regime in which a large strain rate dependence is observed.

CONCLUSION

A new specimen geometry developed recently has been successfully used to investigate the effect of crack velocity on crack arrest fracture toughness in a high strength steel with a ductile failure mode at room temperature. It is shown that K_{Ia} is independent of the crack velocity over the range between 0.1 and 500 m/s.

REFERENCES

(1) Gailly B. and Petit J., "Influence of the microstructure on armor steel spalling", A.P.S. 95, U.S.A., 1995

(2) Iung T., "Propagation rapide et arrêt des fissures dans les aciers pour gazoducs. Rupture par clivage et rupture ductile", Thèse de doctorat, ENSMP, 1994

(3) Henry M., Marandet B., Mudry F. and Pineau A., J. Mec. Théo et Appl., Vol 4, pp 741-768, 1985

(4) Gailly B., "Loi de comportement de trois aciers à blindage", ETBS 005/CT/95, 1995

(5) Di Fant M., "Mécanique et mécanisme de la rupture dynamique dans un acier ferritique peu allié", Thèse de doctorat, ENSMP, 1990

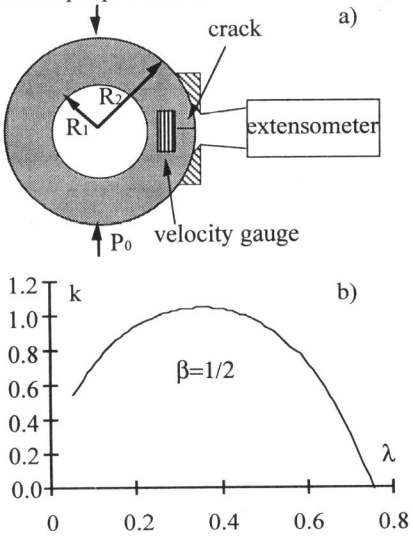

Figure 1 a) Geometry of the ring shape specimen; b) k-λ curve

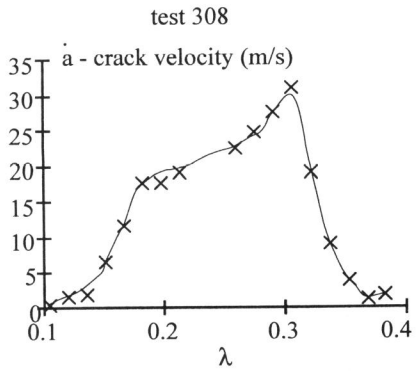

Figure 2 Crack velocity for 308 specimen versus crack length

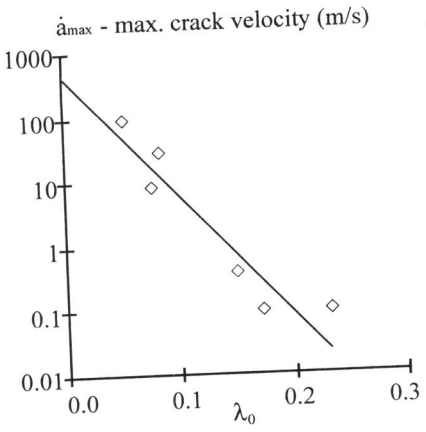

Figure 3 Relation between maximum crack velocity and initial crack length

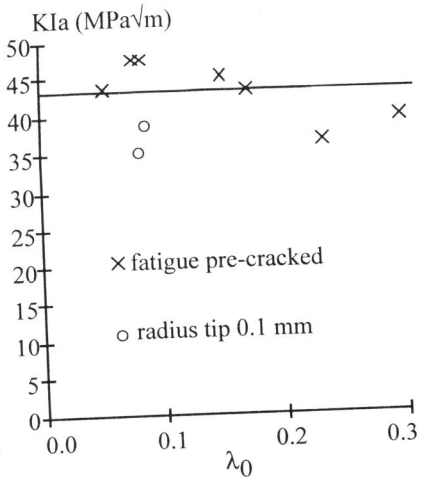

Figure 4 KIa vs initial crack length λ_0

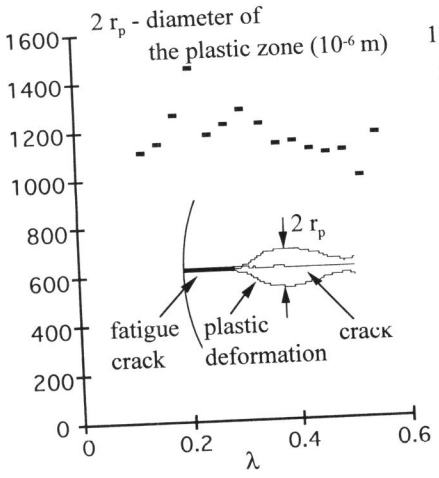

Figure 5 Plastic zone size, 2 r_p, along crack propagation path for 308 test

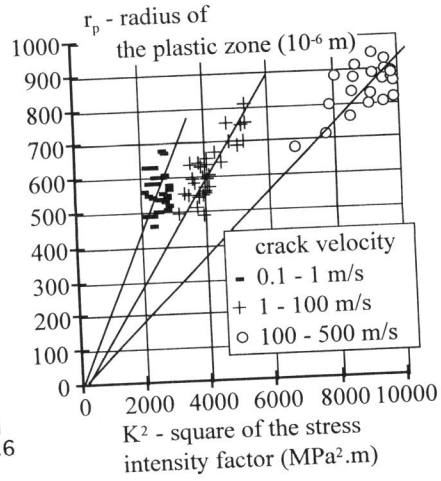

Figure 6 Linear relation between the plastic zone size, r_p, and K^2